AIP | Applied Physics Letters

Traceable atomic force microscopy of high-quality solvent-free crystals of [6,6]-phenyl-C61-butyric acid methyl ester

Giovanni Mattia Lazzerini, Giuseppe Maria Paternò, Giulia Tregnago, Neil Treat, Natalie Stingelin, Andrew Yacoot, and Franco Cacialli

Citation: Applied Physics Letters **108**, 053303 (2016); doi: 10.1063/1.4941227
View online: http://dx.doi.org/10.1063/1.4941227
View Table of Contents: http://scitation.aip.org/content/aip/journal/apl/108/5?ver=pdfcov
Published by the AIP Publishing

Traceable atomic force microscopy of high-quality solvent-free crystals of [6,6]-phenyl-C_{61}-butyric acid methyl ester

Giovanni Mattia Lazzerini,[1] Giuseppe Maria Paternò,[2] Giulia Tregnago,[2] Neil Treat,[3] Natalie Stingelin,[3] Andrew Yacoot,[1] and Franco Cacialli[2]
[1]*National Physical Laboratory, Hampton Road, Teddington, Middlesex TW11 0LW, United Kingdom*
[2]*Department of Physics and Astronomy and London Centre for Nanotechnology, University College London, Gower Street, London WC1E 6BT, United Kingdom*
[3]*Department of Materials Science, Imperial College London, London SW7 2AZ, United Kingdom*

(Received 3 July 2015; accepted 18 January 2016; published online 4 February 2016)

We report high-resolution, traceable atomic force microscopy measurements of high-quality, solvent-free single crystals of [6,6]-phenyl-C61-butyric acid methyl ester (PCBM). These were grown by drop-casting PCBM solutions onto the spectrosil substrates and by removing the residual solvent in a vacuum. A home-built atomic force microscope featuring a plane mirror differential optical interferometer, fiber-fed from a frequency-stabilized laser (emitting at 632.8 nm), was used to measure the crystals' height. The optical interferometer together with the stabilized laser provides traceability (via the laser wavelength) of the vertical measurements made with the atomic force microscope. We find that the crystals can conform to the surface topography, thanks to their height being significantly smaller compared to their lateral dimensions (namely, heights between about 50 nm and 140 nm, for the crystals analysed, vs. several tens of microns lateral dimensions). The vast majority of the crystals are flat, but an isolated, non-flat crystal provides insights into the growth mechanism and allows identification of "molecular terraces" whose height corresponds to one of the lattice constants of the single PCBM crystal (1.4 nm) as measured with X-ray diffraction. [http://dx.doi.org/10.1063/1.4941227]

High-quality, solvent-free crystals of organic semiconductors are essential to the investigation of the physics underpinning the technology of devices such as organic light-emitting diodes (OLEDs), field-effect transistors (OFETs), and photovoltaic diodes (OPVDs).[1,2] In addition, detailed information on the material aggregation behavior, morphology, and electronic properties[3] provides crucial bases for device optimization.

PCBM ([6,6]-phenyl-C61-butyric acid methyl ester), in particular, is one of the most popular choices as the electron acceptor in organic solar cells with type-II heterojunctions. Such architectures are widely used as they favour exciton splitting, both in bilayers[4] and bulk (distributed) heterojunctions (BHJs). In the latter, the interpenetrated electron donor–acceptor network also provides large interface areas and optimizes charge generation.[5,6] Devices based on poly(3-hexylthiophene-2,5-diyl) (P3HT) and PCBM blends display better performance following thermal annealing that alters the fraction of amorphous and microcrystalline PCBM domains,[7,8] with the formation of PCBM nano-crystalline domains that are crucial for high power conversion efficiencies (PCE).[9,10] One of the issues that have hampered progress so far is that the crystal structure of PCBM turns out to be strongly dependent on the solvent in which the crystals are grown and which remain in the crystals themselves as an inclusion. Recently, we have proposed a solution-based procedure to obtain large, solvent-free, high-quality PCBM crystals.[11] This procedure can be carried out at room temperature, avoiding potential reductions in crystal stability or purity caused by thermal annealing.[12] Micro-focused X-ray diffraction (XRD) (I24-Microfocus MX beam-line at Diamond Light Source—UK) showed that PCBM assembles into a monoclinic unit cell ($a = 1.347$ nm, $b = 1.51$ nm, $c = 1.91$ nm) containing four PCBM molecules. Remarkably, the Van der Waals sphere representation indicated that there is not enough space to accommodate a solvent molecule inside the unit cell, and the electron density map from the X-ray diffraction experiments signified that there is no residual solvent present within the voids. Such crystals also display a rich vibrationally resolved low-temperature photoluminescence (PL), afforded by a complex interplay of Herzberg-Teller, Jahn-Teller, and Franck-Condon effects. We refer the reader to Ref. 11 for further details on the crystals' preparation and XRD characterization, and to Ref. 13 for details of the photoluminescence characterization.

Other morphological properties of the crystals are also very important for understanding their fundamental properties and applicative potential, such as their dimensions and the quality (e.g., roughness, defects, etc.) of the crystal surfaces. Such investigations can be pursued, for example, by accurate and traceable dimensional nanometrology, by means of atomic force microscopy.[14–16] To circumvent the problems originating from non-linearity, drift, and hysteresis inherent to piezoelectric transducers (PZTs) in commercial instruments,[17] which result in the voltage conversion being one of the major causes of inaccuracy and lack of traceability, we have used an AFM that has integrated optical interferometry for the measurement of the vertical motion of the PZT tube to compensate for tip bending.[18] Lateral motion is achieved with a high precision dual axis translation stage. Optical interferometry is the primary route to traceability for dimensional metrology, realized in this case by the wavelength of frequency-stabilized He-Ne lasers.[19,20]

Importantly, the use of an optical interferometer decouples the measurement of the Z displacement from the voltage (V_{SL}) applied to the PZT by the servo loop. This therefore prevents errors introduced by associating the V_{SL} to a z displacement when the servo loop compensates for drift or non-linearity of the PZT. The optical interferometer used, the National Physical Laboratory (NPL) Plane Mirror Differential Optical Interferometer (PMDOI),[21] is a homodyne differential interferometer, fiber-fed with a He-Ne frequency-stabilized laser with the wavelength of 632.8 nm.[22]

Measurements of the surface topography were carried out using the AFM in closed-loop, non-contact mode in a temperature-controlled environment ($20\,^{\circ}\text{C} \pm 0.01\,^{\circ}\text{C}$). As well as the PMDOI, the AFM (Fig. 1(a)) uses a fiber interferometer featuring a laser diode ($\lambda = 785$ nm) for detecting the deflection of the cantilever.[18] This is in place of the more usual beam deflection system found in most AFMs. The *total* AFM noise along the z-axis has been measured to be <0.2 nm.[23] The AFM images were numerically corrected for tilt using the "mean plane subtraction" tool in Gwyddion[24] (a freely available software for AFM data visualization and analysis), and the crystal step height was measured according to the international standard ISO 5436 (2000),[25] taking several line profiles (>10) perpendicular to the crystal's long axis and averaging the results. The standard ISO 5436 (2000) defines the currently accepted most accurate way of extracting the step height. The method involves fitting the data taken on the substrate on either side of the single step and on the step itself, and therefore allows any residual tilt of the sample to be removed from the measurement of the step height.

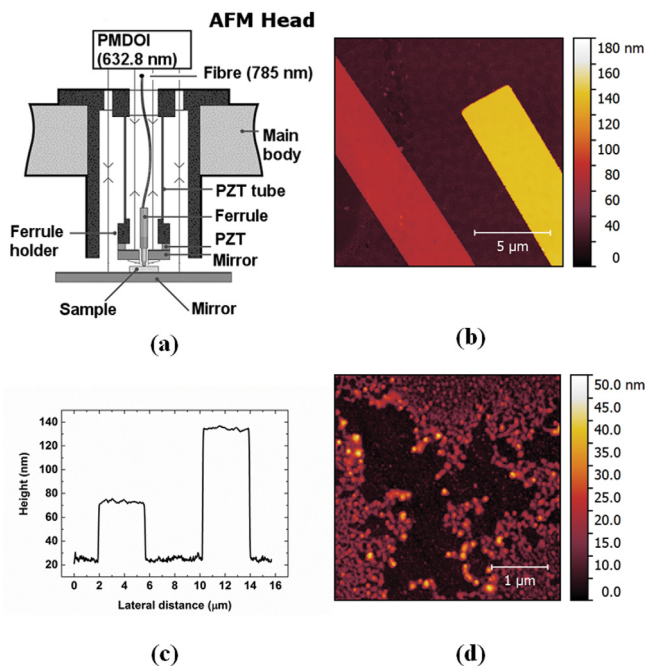

FIG. 1. (a) Schematic of the home-built AFM, including the interferometer beams for the detection of the vertical displacement; (b) AFM image (512 × 512 pixels) and (c) line profile of two PCMB crystals corresponding to the dashed line in Fig. 1(b); (d) AFM measurement (512 × 512 pixels) of the substrate, showing the spectrosil substrate not completely covered by the PCBM agglomerates.

Fig. 1(b) shows an example of the AFM measurements of two PCBM crystals next to one another, on a spectrosil substrate. The measured height averaged along the main axes of the crystal is 48.2 ± 0.9 nm and 109 ± 0.6 nm, respectively (uncertainties here and in the rest of the document are given at one sigma). Fig. 1(b) shows a roughness ("root mean square," rms) of 0.9 nm and 1.0 nm on the lower and higher crystal surfaces, respectively, compared to a roughness of 2.7 nm on the spectrosil substrate. A close-up of the substrate (Fig. 1(d)) also indicates the presence of a non-uniform, discontinuous, 5 nm-thick PCBM layer (reddish grains in Fig. 1(d)) on top of the remaining areas of substrate (black-colored regions in Fig. 1(d)). The roughness of such a non-uniform PCBM layer is 2.9 nm, compared to the 1.4 nm roughness of the spectrosil (slightly different in the close-up compared to the 2.7 nm found on a larger sample of the spectrosil).

Interestingly, several PCBM crystals, measured across multiple samples, showed recurrent height values, multiples of either ~50 nm or ~70 nm (e.g., 49 ± 2 nm and 105 ± 3 nm or 72 ± 2 nm and 139 ± 3 nm). Identification of the factors limiting the growth of the crystals in the vertical direction to specific values is beyond the scope of this work, but, intriguingly, we also note the presence of some overlapping crystals. Fig. 2(a), for example, shows the AFM measurements of two such crystals. Similar to the measurements in Fig. 1, the thickness of the crystal is 106 ± 1 nm and 103 ± 1 nm for both the crystals on the left and the crystal on the right of the image, respectively. The roughness of the non-overlapping areas is 0.6 nm (Figs. 2(c)–2(d)), whereas the top crystal shows a damaged area with "crevices" up to 40 nm deep.

Fig. 3(a) shows the AFM measurements of the only crystal observed that was not flat. From the line profile along the main crystal axis (reported in Fig. 3(b)), the crystal height increases from the edges (63 nm and 81 nm) up to

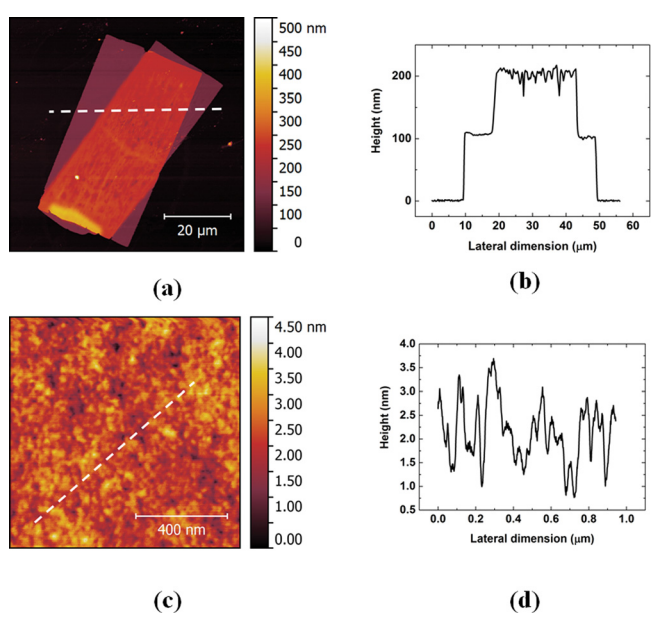

FIG. 2. (a) AFM image (512 × 512 pixels) and (b) line profile of two PCBM crystals with the same height, laying on each other (corresponding to the dashed line in Fig. 2(a)); (c) detailed AFM image (1024 × 1024 pixels) and (d) line profile of the top surface of a PCBM crystal (corresponding to the dashed line in Fig. 2(c)).

210 nm at the center. In addition to recording a surface roughness of 0.6 nm, a "terrace discontinuity" on the crystal surface can be observed in Fig. 3(c) and the value of the step is 1.4 ± 0.2 nm (Fig. 3(d)). The inset of Fig. 3(c) also shows the progression of a few terraces that eventually yield the monotonic increase of the surface morphology towards the center of the long-axis of the crystal. Although the edges of such terraces are relatively rough, it is interesting that they have approximately the same extension in the direction of the crystal long-axis.

We start our discussion from Fig. 1, and note that the crystals are generally rather uniform in thickness, along their length, with deviations of only 0.9 nm and 0.6 nm, respectively, for the ones in this figure, thereby confirming the visual impression of the relatively uniform nature of the crystal surfaces. This complements the information on the high quality of the PCBM crystals as obtained from the XRD measurements, also demonstrating close packing of PCBM within the crystals bulk.[11]

In addition to their uniformity, we observed that the crystals measured can be remarkably thin (thickness as low as 49 nm) compared to their lateral dimensions, which are of the order of few micrometers in width and tens of micrometers in length. Interestingly, the topography measurements (AFM measurement reported in Fig. S1 in the supplementary materials section)[26] show that, thanks to their low thickness, the crystals' form matches that of the underlying substrate. We observed (AFM measurement reported in Fig. S1)[26] that for a non-uniform substrate, the crystals adapt to the surface, and that the morphology of the top surface of the crystal reproduces the one of the substrates underneath the sample.

As a consequence of the slight thickness of these crystals and of their conformability, the measured roughness of the crystal's top surface is given by two components. The first is due to the intrinsic crystal roughness, whereas the second is due to the crystal conforming to the substrate. The actual crystal roughness can thus be lower than the 0.6 nm or 0.9 nm measured. As a confirmation, we also grew crystals on the Si/SiO_2/HMDS (hexametil-disilazane) substrates with roughness <1.2 nm and obtained a crystal surface roughness between 0.3 nm and 0.6 nm (not shown). Such low roughness of the crystals, as measured with the metrological AFM, is also entirely consistent with the highly uniform polarization colors observed in the cross-polarized optical microscopy (reported as Fig. S2 in the electronic supporting information),[26] which are correlated with the actual retardation, birefringence, and thickness of the crystals. Only samples of highly uniform thickness and structural quality will produce such homogenous polarization colors. Furthermore, even with a small misalignment of the crystal with respect to the polarizer and/or analyzer, no complete extinction is observed, further underlying the excellent quality of the produced crystals, as clearly, perfect alignment is needed.

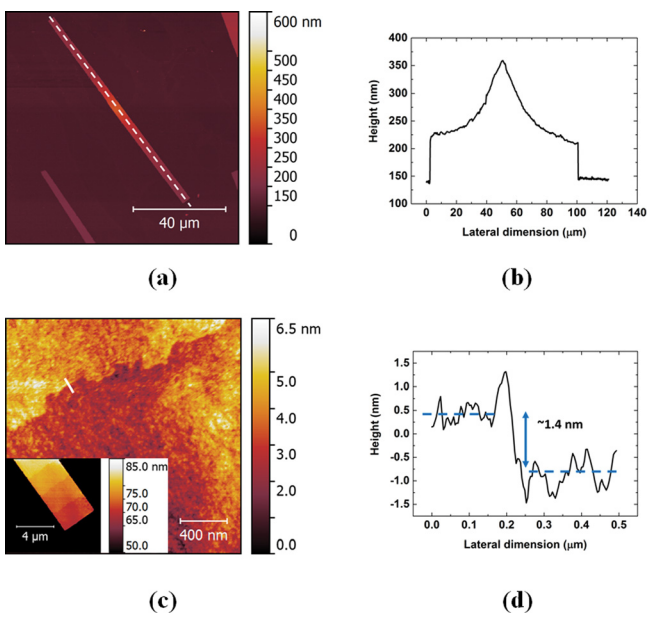

FIG. 3. (a) AFM image (1024 × 1024 pixels) and (b) line profile of a PCBM crystal showing an increasing height from the edges of the crystal towards the center (corresponding to the dashed line in Fig. 3(a)); (c) detailed AFM image (512 × 512 pixels for main figure and 256 × 256 pixels for inset) and (d) line profile of a 1.4 nm step-like defect on the PCBM crystal.

As noted above, from the zoomed-in image (Fig. 1(d)) we also observe the presence of a non-uniform, ~5 nm-thick layer of PCBM. We suggest that during the drying process the PCBM aggregates on the spectrosil substrate, probably clustering around defects in the underlying spectrosil, and these then act as seeds for the formation of the crystals. The formation mechanism of the crystals is still under investigation; however, our data suggest at least two possible mechanisms. First, we propose that the crystals can grow along the directions pointing out of the surface plane, and essentially as part of complex 3D structures which we have also previously reported,[11] and that break (mostly at the base) when the solvent dries out or because of handling. Second, the crystals can also grow horizontally on the substrate on the PCBM layer, i.e., in a direction within the surface plane.

As an indication of the former growth mode, we note, in Fig. 2, two crystals lying on top of one another, and, more generally, the presence of crystals with recurrent height values (e.g., 49 ± 2 nm and 105 ± 3 nm or 72 ± 2 nm and 139 ± 3 nm). We suggest that for these crystals the thickness is a multiple of a given value (~50 nm or ~70 nm) as a consequence of the crystals growing as part of complex stacks,[11] which subsequently collapsed during the drying process. Interestingly, there is a raised area in the bottom part of both crystals in Fig. 2, which lends further support to our interpretation. The crystals appear to have grown simultaneously as a geminate pair from the area of the raised feature, and then the one lying on the top was later broken, collapsing on the other crystal, thereby leaving a "stump" (raised area). Fig. 2(a) also shows the presence of several defects on the area where the crystals overlap, but not outside of it. We consider that such defects have been generated by the evaporation of the solvent trapped between the two crystals, which must have found its way through the upper crystal, and thereby leaving it damaged owing to the fast solvent evaporation upon exposure to vacuum.

A different crystal formation mechanism is necessary to explain the unique shape reported in Fig. 3(a). Here, we propose that the crystal was formed by the evaporation of a drop of solution that retracted towards the center as the solvent evaporated, thus leading to a progressively higher PCBM concentration in the droplet which in turn deposited an

increasingly larger amount of material when progressing towards the center of the crystal. A corroborating indication of this is the presence of (already noted) several terraces perpendicular to the main crystal axis illustrated in the inset of Fig. 3(c). Interestingly, the step height is $1.4\,\text{nm} \pm 0.2\,\text{nm}$, which corresponds to the "a" lattice constant (1.347 nm), as measured recently via single-crystal XRD.[11] We therefore propose that the measured step is generated as the drop retracts, laying a new crystal plane on top of the existing ones.

In conclusion, we presented high resolution, traceable AFM measurement of high quality PCBM crystals. The crystals were grown via slow-evaporation of a solvent but, as reported previously, they showed no solvent inclusion after vacuum exposure. The effect of the drying process has been considered for understanding the damage in limited areas of crystals and the formation of $\sim$1.4 nm step terrace-like defects corresponding to the crystal lattice constant. Traceable AFM measurements confirmed that the roughness of the crystals' surfaces can be as low as 0.6 nm (or 0.3 nm depending on substrates), which, together with their high quality bulk structure, make them good candidates for further investigations of the basic physical properties of this important and intriguing material.

We thank Dr. Anna Warren from the Diamond Light Source in the UK for helpful discussions, the EC Seventh Framework Programme (FP7/2007-2013) under Grant Agreement No. 264694 (GENIUS), the EU Horizon 2020 Research and Innovation Programme under Grant Agreement No. 643238 (SYNCHRONICS), as well as the Royal Society and the EPSRC. G.M.P. was supported by an IMPACT Ph.D. studentship co-sponsored by UCL and ISIS-Neutron and Muon Facility (Science and Technology Facilities Council). This research was also supported by the European Union by funding the European Metrology Research Programme (EMRP) Project "Traceable measurement of mechanical properties of nano-objects (MechProNo)." The EMRP is jointly funded by the EMRP participating countries within the EURAMET and the European Union. F.C. is a Royal Society Wolfson Research Merit Award holder.

[1]V. Podzorov, MRS Bull. **38**(1), 15 (2013).
[2]A. L. Briseño, S. C. Mannsfeld, M. M. Ling, S. Liu, R. J. Tseng, C. Reese, M. E. Roberts, Y. Yang, F. Wudl, and Z. Bao, Nature **444**(7121), 913 (2006).
[3]B. A. Collins, J. R. Tumbleston, and H. Ade, J. Phys. Chem. Lett. **2**(24), 3135 (2011).
[4]A. L. Ayzner, C. J. Tassone, S. H. Tolbert, and B. J. Schwartz, J. Phys. Chem. C **113**(46), 20050 (2009).
[5]G. Yu, J. Gao, J. C. Hummelen, F. Wudl, and A. J. Heeger, Science **270**(5243), 1789 (1995).
[6]J. J. M. Halls, C. A. Walsh, N. C. Greenham, E. A. Marseglia, R. H. Friend, S. C. Moratti, and A. B. Holmes, Nature **376**(6540), 498 (1995).
[7]G. Paternò, F. Cacialli, and V. García-Sakai, Chem. Phys. **427**, 142 (2013).
[8]W. Yin and M. Dadmun, ACS Nano **5**(6), 4756 (2011).
[9]M. T. Rispens, A. Meetsma, R. Rittberger, C. J. Brabec, N. S. Sariciftci, and J. C. Hummelen, Chem. Commun. **2003**(17), 2116 (2003).
[10]Y. Kim, J. Nelson, T. Zhang, S. Cook, J. R. Durrant, H. Kim, J. Park, M. Shin, S. Nam, M. Heeney, I. McCulloch, C. S. Ha, and D. D. Bradley, ACS Nano **3**(9), 2557 (2009).
[11]G. Paternò, A. J. Warren, J. Spencer, G. Evans, V. G. Sakai, J. Blumberger, and F. Cacialli, J. Mater. Chem. C **1**(36), 5619 (2013).
[12]M. Casalegno, S. Zanardi, F. Frigerio, R. Po, C. Carbonera, G. Marra, T. Nicolini, G. Raos, and S. V. Meille, Chem. Commun. **49**(40), 4525 (2013).
[13]G. Tregnago, M. Wykes, G. M. Paternò, D. Beljonne, and F. Cacialli, J. Phys. Chem. C **119**(21), 11846 (2015).
[14]G. Binnig, C. F. Quate, and C. Gerber, Phys. Rev. Lett. **56**(9), 930 (1986).
[15]H. U. Danzebrink, L. Koenders, G. Wilkening, A. Yacoot, and H. Kunzmann, CIRP Ann. Manuf. Technol. **55**(2), 841 (2006).
[16]F. Giessibl and E. Vi, Rev. Mod. Phys. **75**(3) 949 (2003).
[17]A basic atomic force microscope (AFM) consists of a cantilever, with a sharp tip at its end, raster-scanned on the surface under test. Recalling the well-known working principle of an AFM, the presence of features on the surface induces bending in the cantilever or a variation of its oscillation amplitude if the AFM is working in contact or non-contact mode, respectively, and such changes can be related to the height of surface features. By operating the AFM in closed-loop, the bending of the cantilever or the variation of its oscillation amplitude is compensated by moving the entire cantilever vertically using a piezoelectric transducer (PZT). On many commercial systems, the vertical displacement, and therefore the surface topography, is obtained by converting the voltage applied to the PZT into displacement. Considering the non-linearity, drift and hysteresis inherent to PZTs, the voltage conversion is one of the major causes of inaccuracy and lack of traceability. Even after calibration, the PZT is still subject to hysteresis non-linearity, and if the sample is tilted, the z measurement range will be greater than the sample height. Any calibration of a conventional AFM will be based on a calibration standard that will have been calibrated using a metrological AFM (i.e., an AFM with an interferometer) as the one used here. As a consequence, the uncertainty resulting from the calibration will be greater than that of the interferometer-based AFM. We confirm that the AFM that we used for these measurements has indeed been used to calibrate step height standards that are used to calibrate other AFMs.
[18]A. Yacoot, L. Koenders, and H. Wolff, Meas. Sci. Technol. **18**(2), 350 (2007).
[19]M. Pisani, A. Yacoot, P. Balling, N. Bancone, C. Birlikseven, M. Celik, J. Flugge, R. Hamid, P. Kochert, P. Kren, U. Kuetgens, A. Lassila, G. B. Picotto, E. Sahin, J. Seppa, M. Tedaldi, and C. Weichert, Metrologia **49**(4), 455 (2012).
[20]J. A. Stone, J. E. Decker, P. Gill, P. Juncar, A. Lewis, G. D. Rovera, and M. Viliesid, Metrologia **46**(1), 11 (2009).
[21]A. Yacoot and M. J. Downs, Meas. Sci. Technol. **11**(8), 1126 (2000).
[22]The PMDOI traceably measures the relative displacement between the tip and the sample by using the interference of two optical paths. Such paths are defined by beams reflected twice on two parallel mirrors. One mirror is rigidly connected to the PZT tube that moves the cantilever, and the other forms the sample holder. Since the beams in each path are reflected twice on the relevant mirror, the sensitivity of the interferometer is doubled, and each fringe corresponds to $\lambda/4$ or $\sim$158 nm for the He-Ne laser used here. The theoretical resolution of the interferometer is better than 10 pm, but we note that what is important is the accuracy of the instrument (deviation from correct value) rather than resolution or precision. We measured that the noise level of the instrument is <0.2 nm (when operating in closed loop) and this is the source of inaccuracy.
[23]For the noise measurement, the AFM was operated in closed loop to keep the tip in contact with a flat substrate and the tip kept stationary (not scanning). Transient measurements of the z displacement (measured with the interferometer) of the tip were recorded over times ranging from 100 ms to 30 s. FFT of the measurements were performed and the noise was extracted.
[24]D. Nečas and P. Klapetek, Cent. Eur. J. Phys. **10**(1), 181 (2011).
[25]ISO 5436-1:2000, *Geometrical Product Specifications (GPS)—Surface Texture: Profile Method; Measurement Standards—Part 1: Material Measures* (ISO, 2000).
[26]See supplementary material at http://dx.doi.org/10.1063/1.4941227 for further details of the influence of the substrate on the crystal surface roughness and of polarised optical microscopy.